Heliyon 10 (2024) e34046

Contents lists available at ScienceDirect

Heliyon

journal homepage: www.cell.com/heliyon

Research article

Oxidative stress-related genes score predicts prognosis and immune cell infiltration landscape characterization in breast cancer

Diya Liu, Lin Fang *

Department of Thyroid and Breast Surgery, Shanghai Tenth People's Hospital, School of Medicine, Tongji University, Shanghai 200072, China

ARTICLE INFO

Keywords:
Oxidative stress
Oxidative stress-related genes
Breast cancer
Immune cell infiltration
Tumor progression

ABSTRACT

Background: The tumor microenvironment (TME) typically experiences oxidative stress (OS), marked by a high level of reactive oxygen species (ROS) that can impact tumor advancement and prognosis by modulating the behavior of tumor cells and various immune cells. Oxidative stress-related genes (OSRG) encompass a range of genes involved in ROS pathways, and their specific roles in breast cancer (BC) necessitate further investigation.

Methods: Univariate Cox analysis was performed on genes linked to the OS pathway in the Gene Set Enrichment Analysis (GSEA) database, leading to the identification of 29 significant OSRG in BC. OSRG was divided into three distinct clusters according to the expression and the OSRG score based on the differentially expressed genes (DEGs) was further calculated by principal component analysis (PCA). The correlation between OSRG score and BC clinical features, mutation characteristics, immune checkpoints and immune cell infiltration was analyzed. Establish a multiariable Cox regression model to predict OSRG score effects on clinical characteristics.

Results: Significant differences were observed in survival analysis, enriched pathways, and immune infiltration among the three OSRG clusters based on 29 genes. Gene clusters were identified through the final selected 395 DEGs, revealing three distinct OSRG expression patterns. An OSRG score model was constructed using DEGs, demonstrating a significant association between high OSRG score and poor prognosis. Significantly, immune checkpoint-related genes exhibited a notable upregulation in the high OSRG score cohort. Additionally, a positive correlation was observed between the OSRG score and tumor mutation burden (TMB) in BC. The OSRG score holds potential implications for clinical immunotherapy in BC patients, and a nomogram was constructed with robust predictive capability for evaluating patient prognosis.

Conclusions: This study elucidated the features of OSRG within BC TME and their possible prognostic significance, offering valuable insights for the development of more targeted immunotherapy approaches for individuals with BC.

1. Introduction

The incidence of BC is steadily increasing each year, making it the primary cause of morbidity and the second leading cause of mortality among women [1]. According to the most recent global Cancer burden data for 2023 released by the International Agency for

* Corresponding author.
E-mail address: 1200038@tongji.edu.cn (L. Fang).

https://doi.org/10.1016/j.heliyon.2024.e34046
Received 26 April 2024; Received in revised form 25 June 2024; Accepted 2 July 2024
Available online 4 July 2024

Research on Cancer (IARC), the prevalence of female BC has shown a gradual annual rise of approximately 0.5 % since the mid-2000s [2]. While breast cancer therapies encompass surgical procedures, endocrine therapy, targeted therapy, chemotherapy, and radiotherapy, they are nevertheless subject to several limitations. These include the heterogeneity of the illness due to individual variations and the less-than-ideal treatment outcomes. Genomic research plays a crucial role in precision medicine, which aims to produce personalized treatment for breast cancer patients [3].

ROS and reactive nitrogen species (RNS) are overproduced in the body in response to harmful stimuli, causing an imbalance between oxidative and antioxidant mechanisms. This imbalance leads to tissue damage, known as OS [4]. ROS are known to play critical roles in a wide range of physiological processes, such as immune responses, cell proliferation, and intracellular signaling pathways [5].

The involvement of OS in tumorigenesis, tumor progression, and prognosis is increasingly recognized, with cancer cells often exhibiting heightened susceptibility to ROS and disrupted REDOX homeostasis [6,7]. OS and hypoxia can modulate the metabolic reprogramming of the TME, influencing key metabolic enzymes and perturbing REDOX equilibrium [8]. Additionally, OS-induced DNA damage is closely associated with all stages of carcinogenesis [9]. Notably, OS within the TME can foster immunosuppression by promoting the infiltration of myeloid-derived suppressor cells (MDSCs), thereby impeding host anti-tumor immunity [10]. The impact of OSRG on BC pathogenesis may also extend to influencing the tumor immune microenvironment.

Through the establishment of an OSRG score derived from 29 significant OSRGs in BC, our investigation utilized GSEA to explore the relationship between the OSRG score and the infiltration of immune cells, mutation profiles, and clinical attributes in BC. Our results provide insights into the unique characteristics of OSRGs in the BC microenvironment and their potential prognostic relevance, thereby contributing valuable knowledge for the advancement of more effective immunotherapeutic approaches for BC patients.

2. Materials and methods

2.1. BC dataset source and preprocessing

The workflow of our study was shown in Fig. S1. OS pathways and associated genes were identified through GSEA database (https://www.gsea-msigdb.org/gsea/msigdb/human/geneset/GOBP_RESPONSE_TO_OXIDATIVE_STRESS), leading to the selection of 29 OSRGs through univariate Cox analysis (**Table Supplementary 1**). A total of 1091 BC samples from The Cancer Genome Atlas (TCGA) database (https://portal.gdc.cancer.gov) and 99 BC samples from the International Cancer Genome Consortium (ICGC, https://dcc.icgc.org/) were included in the study. Clinical data, immune cell infiltration, and somatic mutation information were also gathered. The removal of batch effects from gene expression data was performed using the R "Combat" method [11].

2.2. The estimation of immune infiltration and unsupervised clustering for OSRG

The infiltration levels of various immune cells in BC were quantified using the CIBERSORT method, which employed LM22 labeling and 1000 permutations for analysis [12]. Samples with CIBERSORT output of $P < 0.05$ were further analyzed (perm = 100). 29 OSRGs were utilized to delineate distinct ORSG patterns in BC. R "ConsensusClusterPlus "was used to apply unsupervised cluster analysis to identify diverse OSRG patterns for stratifying BC patients, facilitating subsequent analyses. To make sure that the clusters that were identified were robust, this iterative process was performed 500 times [13,14].

2.3. DEGs associated with the OSRG phenotype

To filter the DEGs from the three created OSRG clusters, R "limma" was employed. The corrected P values were scrutinized at to correct false-positive TCGA data. The cutoff values were established as $|\text{Log fold-change}| > 1$ and $P < 0.05$ (adjusted). Use the online database (https://david.ncifcrtf.gov/) of the DAVID (the Database for Annotation, Visualization and Integrated Discovery) for the GO/KEGG enrichment analysis of the above-mentioned DEGs.

2.4. Generation of OSRG score

We developed a scoring system, which named OSRG score, based on DEGs to assess the OSRG model of individual BC patients. The following are the steps to determine the OSRG score: Initially, the overlapped genes were collected and the DEGs between the three created OSRG clusters were normalized. Based on overlapping DEGs, a technique known as unsupervised clustering was utilized to divide BC patients into many groups. A consensus clustering approach was employed to ascertain the quantity of gene clusters and their stability. Subsequently, we conducted prognosis assessments for each gene in the signature utilizing univariate Cox regression models. Genes of prognostic significance were isolated for further investigation. Principal component analysis (PCA) was conducted to create gene features connected to OSRG. The signature scores were chosen as principal components 1 and 2.

Subsequently, we established the OSRG score by employing a methodology akin to that of GGI [15,16].

$$OSRG\ score = \sum PC1_i + \sum PC2_i$$

Where i is the expression of overlapped genes.

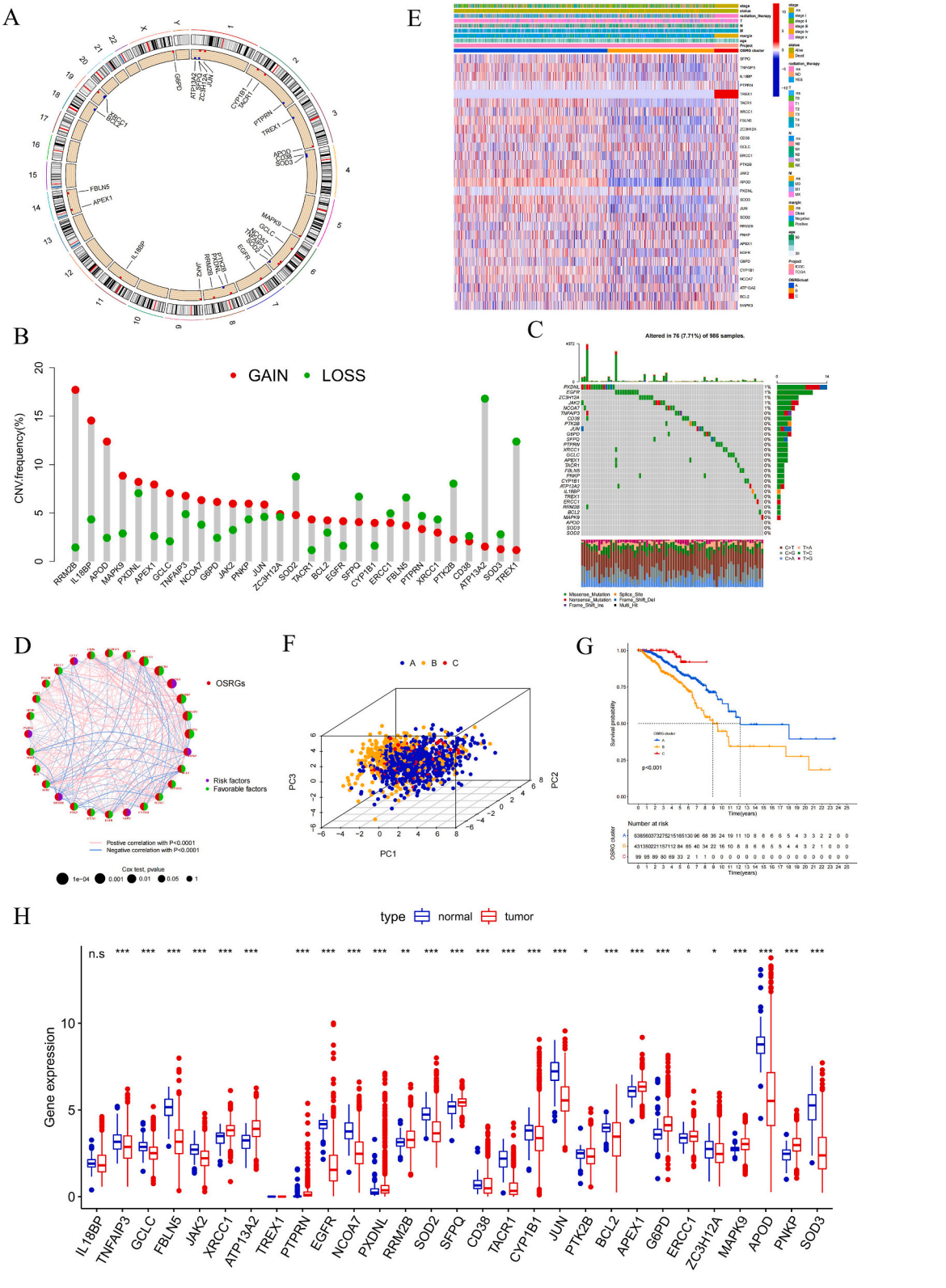

(caption on next page)

Fig. 1. Landscape of genetic and expression variation of OSRG in BC. (A) The location of CNV alteration of OSRG in chromosomes. (B) The CNV variation frequency of OSRG in BC. (C) The mutation frequency of 29 OSRG in 986 BC patients. (D) Single-factor cox analysis of the interaction between OSRG in BC. (E) PCA for the expression profiles of OSRG. (F) The 29 OSRG' expression in 3 OSRG clusters. Rows represent OSRG, columns represent different clinical characteristics. (G) K-M plot was executed to explore OS rate of three OSRG clusters in BC. (H) The differential expression of 29 OSRG between BC tissues and normal tissues. ns represents no statistics differences, * represent $P < 0.05$, ** represent $P < 0.01$, *** represent $P < 0.001$.

2.5. Somatic mutation analysis

This study obtained somatic mutation data for BC samples using the UCSC Xena browser. The TMB of each patient was determined by counting the total number of non-synonymous mutations in BC. A waterfall plot was conducted using R "Maftools" to categorize the BC samples into groups based on their OSRG scores, namely high OSRG score groups and low OSRG score groups [17]. Further analysis was conducted on the top 20 genes with the highest mutation frequency.

2.6. Construction and validation of a predictive nomogram

The prediction capability of the OSRG score was enhanced by utilizing a nomogram constructed using clinical data from TCGA-BRCA. Inclusion criteria encompassed tumor margin, OSRG score, patient age, tumor stage, and additional pertinent clinical factors. The nomogram was verified using a calibration procedure.

2.7. Statistical analysis

R version 4.0.5 was utilized for conducting all statistical analyses. In this study, the Wilcoxon test was employed to compare two groups, whereas the Kruskal-Wallis test was utilized to compare several groups. The survival curve was constructed using the Kaplan-Meier (K-M) method. The statistical significance of the discrepancies was assessed using the log rank test. The correlation between OSRG score subgroups and somatic mutation frequency was analyzed using the χ 2 test, while the correlation coefficient was calculated using Spearman analysis. A significance level of 0.05 was deemed statistically significant in a two-tailed test.

3. Results

3.1. Landscape of genetic and expression variation of OSRG in BC

In this study, a total of 29 OSRGs were examined. The analysis focused on copy number variation and mutation frequency of these genes in BC. A schematic representation of the locations of copy number variants (CNV) on the chromosomes of the genes involved is presented in Fig. 1A. CNV variants were found to be prevalent in the 29 OSRG, with SOD2, SFPQ, FBLN5, PTK2B, ATP13A2, and TREX1 commonly deleted. Most other genes exhibited copy number amplification, with RRM2B showing particularly notable amplification (Fig. 1B). Mutation frequency analysis of the 29 OSRG in 986 BC patients from the TCGA mutation dataset revealed mutations in 76 patients, with a frequency of 7.71 %. The most frequently mutated genes were PXDNL, EGFR, ZC3H12A, and JAK2, while other genes showed minimal mutation rates (Fig. 1C).

Univariate Cox analysis and co-expression analysis of OSRG-related genes constructed the OSRG gene regulatory network, showing the interaction, interconnection among OSRG and their prognostic significance for BC patients (Fig. 1D), using Pearson to calculate their relevance. PCA was conducted in Big Data utilizing the OSRG transcriptome data from the TCGA database. The analysis of ConsensusClusterPlus package revealed that the Delta area exhibited inflection points at a cluster size of 3. By evaluating the slope of the consensus cumulative distribution function, a cluster size of 3 was determined to be the optimal k value. The consensus matrix revealed that the coherence of each group was most pronounced when the group was partitioned into three distinct subgroups (Fig. S2, Table Supplementary 2). We conducted an analysis of the expression of three OSRG clusters in each sample using transcriptome data from TCGA and ICGC databases (Fig. 1E). Fig. 1F and Fig. S3 depict the three groups from both three-dimensional (3D) and planar viewpoints. Significant disparities in survival analysis were observed when the data was divided into three groups. Group B showed the most pronounced disadvantage in terms of survival (Fig. 1G). The study proceeded to examine the expression levels of OSRG between BC tumor tissues and normal tissues. The results indicated that the majority of OSRG expression differences were statistically significant (Fig. 1H). The aforementioned data indicates that the dysregulation of OSRG expression in BC tissues may have a significant impact on the advancement of BC.

3.2. Genes' expression and TME cell infiltration characteristics in distinct OSRG clusters

The researchers employed the GSVA enrichment analysis to evaluate the enrichment routes of the three clusters. Pairwise comparisons revealed that the difference between the enrichment pathways of Cluster-A and Cluster-B was the most significant (Fig. 2A). Cluster-B shown a notable propensity for pathways linked to cell cycle and genetic material modification, including cell cycle, homologous recombination, RNA degradation, mismatch repair, and nucleotide excision repair. Conversely, Cluster-A revealed a contrasting pattern (Fig. 2A).

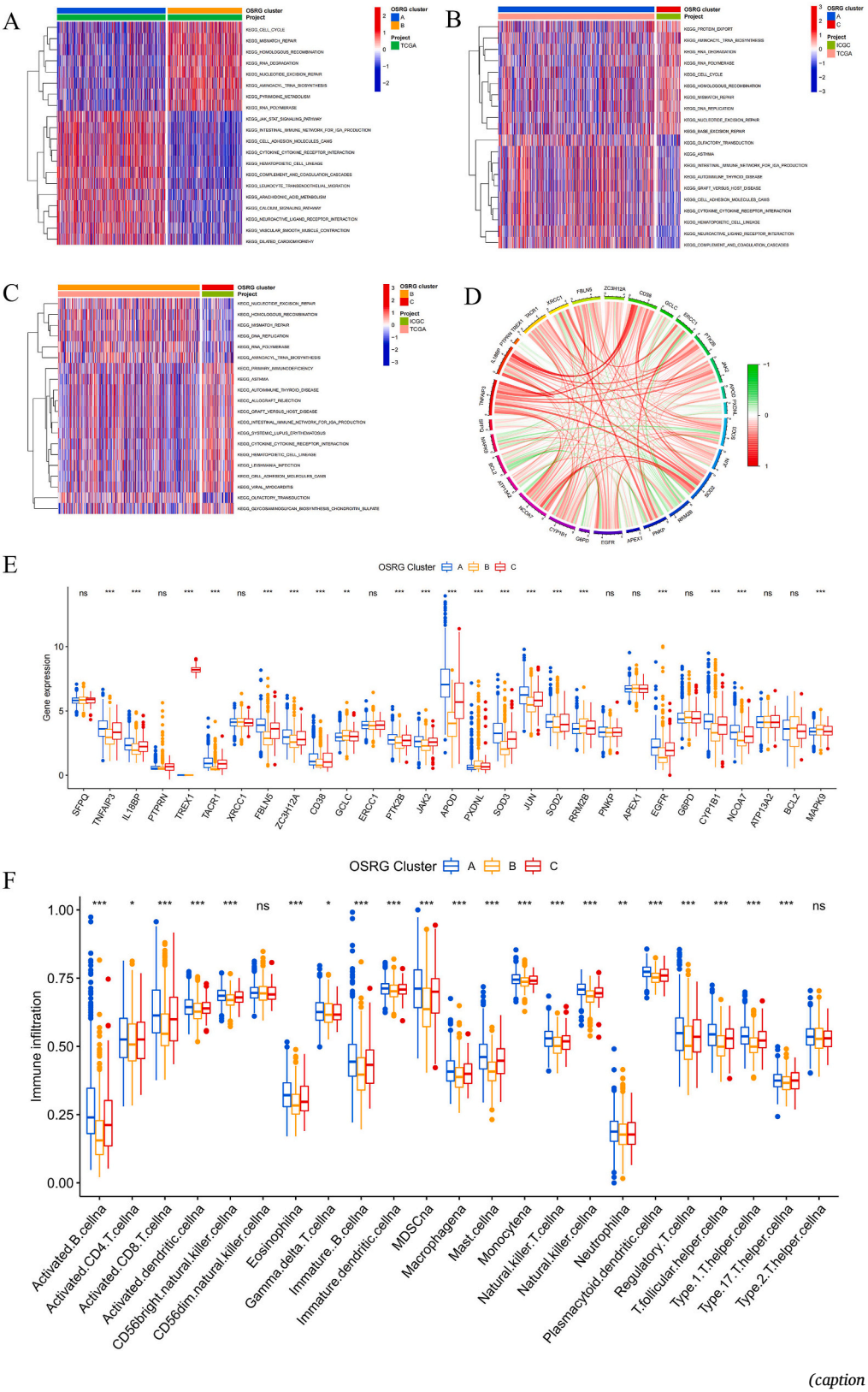

(caption on next page)

Fig. 2. Genes' expression and TME cell infiltration characteristics in distinct OSRG clusters. (A–C) GSVA enrichment analysis of biological pathways in distinct OSRG clusters (Cluster-A vs Cluster-B, Cluster-A vs Cluster-C, Cluster-B vs Cluster-C). (D) Co-expression relationship between OSRG. (E) The expression of OSRG in 3 gene clusters. (F) Immune cell difference infiltration among 3 distinct gene clusters. ns represents no statistics differences, * represent $P < 0.05$, ** represent $P < 0.01$, *** represent $P < 0.001$.

There were additional differences in enrichment pathways detected between Cluster-A and Cluster-C, as well as between Cluster-C and Cluster-B, but these differences were less pronounced (Fig. 2B and C). Fig. 2D illustrates the co-expression connections observed among OSRG genes. Genes in the three clusters exhibited consistent variations in expression levels among the groups (Fig. 2E). Using R "CIBERSORT" to calculate the proportions of immune cell types in the BC samples, analysis the immune cells in OSRG infiltrating differences between three OSRG groups (**Table Supplementary 3**). The infiltration of innate immune cells, such as T cells, dendritic cells, B cells, natural killer cells, eosinophils, and MDSC, was shown to be more numerous in Cluster-A and Cluster-C. The observed immune infiltration demonstrated a comparable survival benefit (Fig. 2F).

3.3. Reconstruction of OSRG clusters based on DEGs

To further optimize the typing of tumor clusters and reduce noise and redundancy, and to further reveal the biological characteristics of breast cancer related to different OSRG phenotypes, We obtained 1170 DEGs (Fig. S4, Table Supplementary 4) and then selected 395 genes (**Table Supplementary 5**) that were significantly different in all three clusters A, B, and C for more accurate analysis. Unsupervised clustering was performed on TCGA and ICGC database cohorts comprising 1190 BC samples, revealing three distinct OSRG expression patterns denoted as OSRG-DEG clusters A, B, and C (Fig. 3A). This clustering approach was determined to be optimal using the ConsesusCluster Plus package (Fig. S5). PCA analysis showed that the clustering based on DEGs could more effectively distinguish OSRG (Fig. 3B, Fig. S6). The results of the survival analysis revealed that OSRG-DEG cluster A demonstrated the lowest overall survival rate (Fig. 3C). The functional enrichment analysis conducted using DAVID demonstrated that DEGs exhibited considerable enrichment in pathways linked to immunological activation and components involved with the cell membrane (Fig. 3D and E). Fig. 3F illustrates the differential gene expression profiles of OSRG within the three OSRG-DEG clusters. Afterwards, the presence of 23 different types of immune cells in the three OSRG-DEG clusters was evaluated. OSRG-DEG cluster C showed the infiltration of innate immune cells and activation of the stroma, while OSRG-DEG cluster A exhibited characteristics of immunosuppression (Fig. 3G).

3.4. Generation of OSRG score

PCA was utilized to compute the OSRG score. The alluvial diagram depicts the gene modules of the two clusters mentioned above, as well as the distribution of patients with high and low OSRG scores (Fig. 4A). The high and low OSRG scores were distinguished according to the optimal cutoff value (best cut-off value = 8.552051). The particular OSRG scores for each sample are provided in **Table Supplementary 6**. The OSRG score was used to stratify the TCGA and ICGC cohorts. The survival analysis revealed a significant correlation between a high OSRG score and a poorer prognosis, while a low OSRG score was associated with a good outcome (Fig. 4B). Fig. 4C presents a heat map that illustrates the predominant topography of immunological interactions inside the TME in BC. 160 DEGs were found in both high and low OSRG scores (Fig. 4D, Table Supplementary 7). Significant differences in OSRG scores were seen among OSRG clusters and OSRG-DEG clusters, as indicated by the results of the Kruskal-Wallis test (Fig. 4E and F). We performed a randomized internal validation to verify the stability of this OSRG score (Figs. S7 and S8).

3.5. Validation of OSRG score and its role in TMB

GSEA analysis revealed that pathways enriched in the high OSRG score group included oxidative phosphorylation and DNA repair, while the low OSRG score group showed enrichment in P53, Wnt-βcatenin signaling, and inflammatory response pathways (Fig. 5A). Furthermore, a comparison between survival and death cases demonstrated significantly lower OSRG scores in survival cases (Fig. 5B); however, the OSRG score did not exhibit clear discriminatory ability between tumor grades (Fig. 5C).

Furthermore, a correlation analysis was performed to examine the relationship between 13 immunological examination sites and the OSRG score. The results showed that all genes associated to immune checkpoints showed considerable overexpression in the group with a high OSRG score (Fig. 5D). The aforementioned research provides a fundamental basis for prospective clinical applications in the field of immunotherapy. The TCGA-BRCA cohort further examined the impact of TMB on individual responses to cancer immunotherapy (**Table Supplementary 8**). The patients were divided into two groups based on their TMB levels: high and low. Survival analysis revealed that high TMB was linked to worse outcomes (Fig. 5E). Fig. 5F and G demonstrate a notable positive association between the OSRG score and TMB.

The possible synergistic impact of the OSRG score and TMB level on the prognosis of BC was further evaluated. The stratified survival analysis showed that the high OSRG score and high TMB group had the worst survival results, whereas the low OSRG score and low TMB group had the opposite outcome (Fig. 5H). The integration of the OSRG score and TMB level has the potential to provide improved prediction accuracy for BC prognosis. Finally, the maftools software program was employed to analyze the proportion of somatic variations among the high and low OSRG score groups in the TCGA-BRCA cohort. Fig. 5I and J (Fig. S9) illustrate the mutation distribution profiles of the top 20 driver genes exhibiting the highest mutation frequencies.

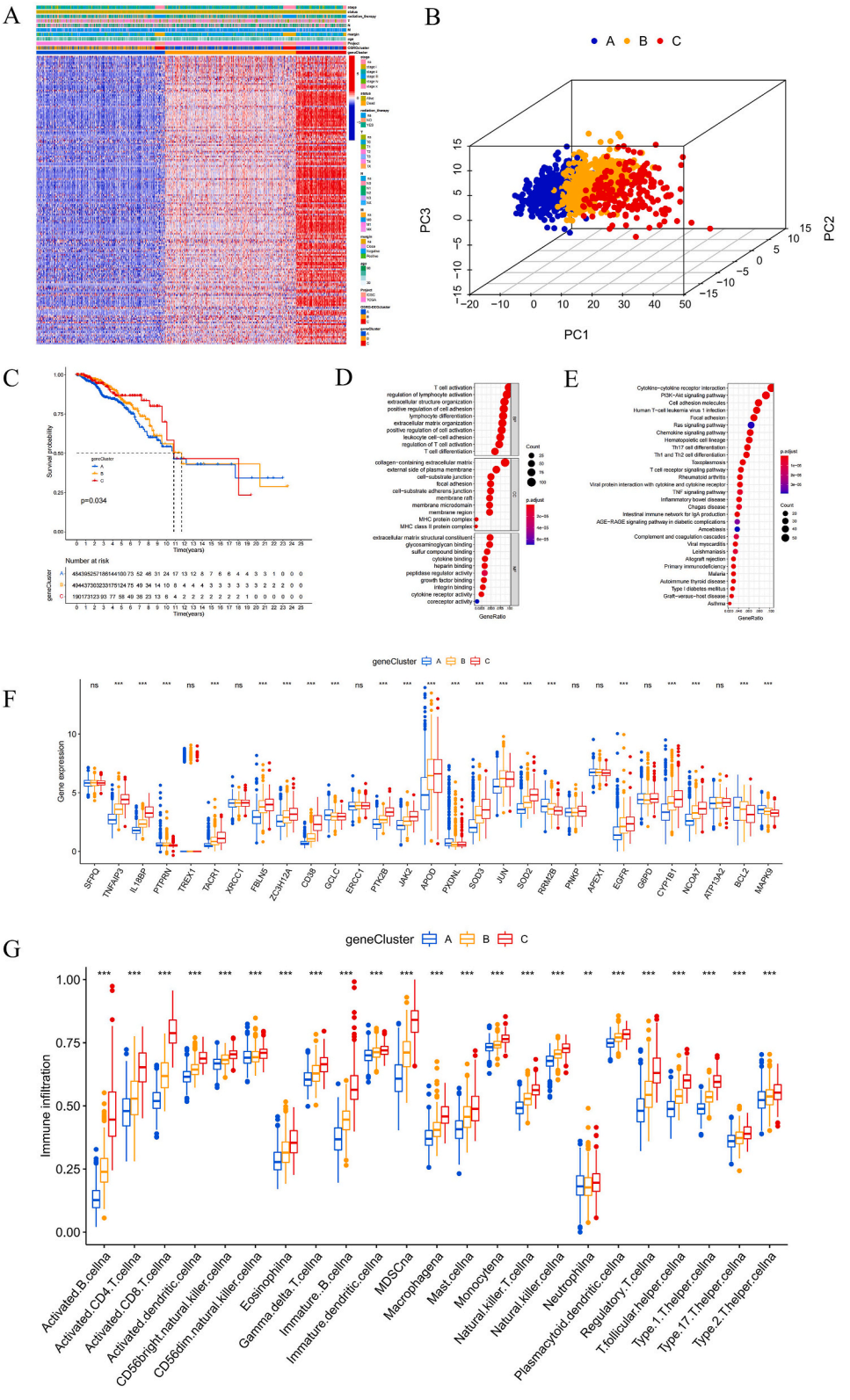

(caption on next page)

Fig. 3. Reconstruction of OSRG clusters based on DEGs in BC samples. (A) The heatmap of the distribution of 1170 DEGs among 3 OSRG-DEG clusters. (B) PCA of 3 OSRG-DEG clusters. (C) K-M curves was executed to explore OS rate of 2 gene clusters in BC (log-rank test $P < 0.05$). (D) The GO analysis of DEGs. (E) The KEGG analysis of DEGs. (F) The expression of OSRG in 3 OSRG-DEG clusters. (G) Immune cell difference infiltration among 3 distinct gene clusters. ns represents no statistics differences, * represent $P < 0.05$, ** represent $P < 0.01$, *** represent $P < 0.001$.

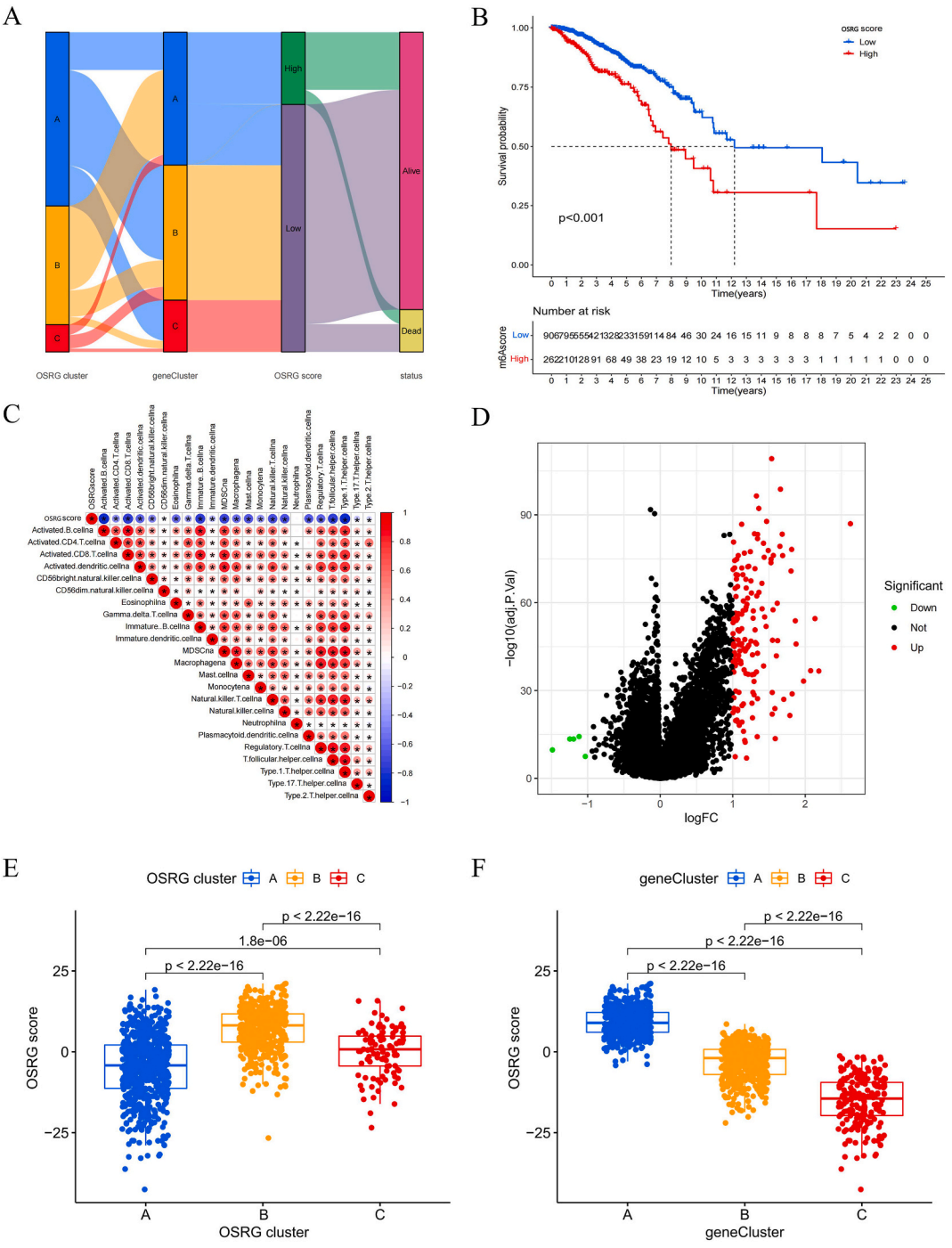

Fig. 4. Establishment of the OSRG score pattern. (A) Alluvial diagram performed the distribution of BC within OSRG cluster, OSRG-DEG clusters, OSRG score, and overall survival status. (B) K-M plot analysis was executed to reveal the prognosis of OSRG score pattern ($P < 0.001$). (C) Correlations between OSRG score and the immune cell infiltration using Spearman analysis. (D) DEGs analysis of high and low OSRG score. (E) The OSRG score in 3 distinct OSRG clusters. (F) The OSRG score in 3 distinct OSRG-DEG clusters.

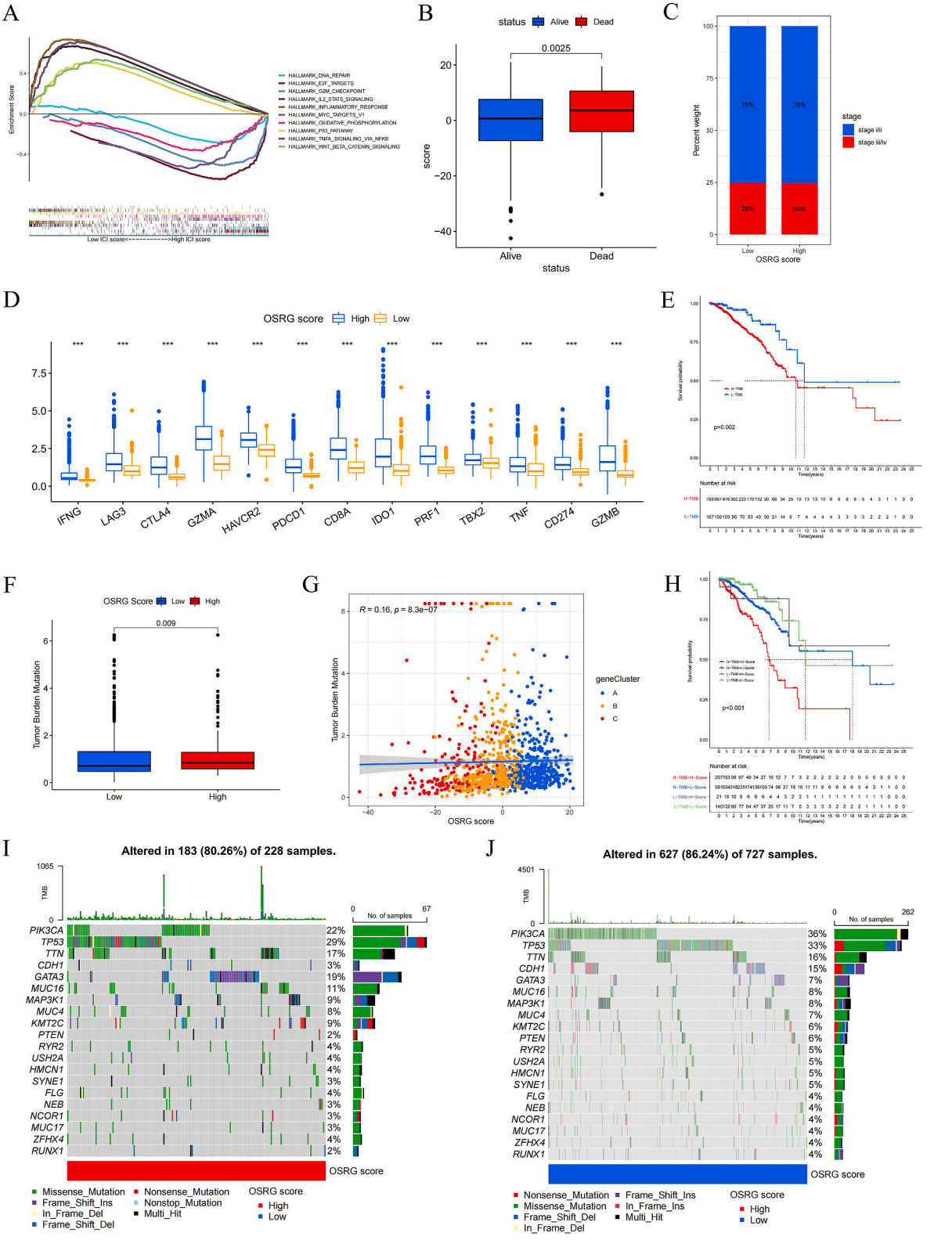

(caption on next page)

Fig. 5. Validation of OSRG score and its role in TMB in BC. (A) GSEA analysis of enriched pathways with high OSG score and low OSG score. (B) Analysis of differences in OSRG score in survival and death cases. (C) Differential analysis of OSRG score in tumor staging. (D) The correlation between OSRG score and immune check points in BC. (E) K-M plot analysis was executed to reveal the prognosis of TMB pattern ($P = 0.002$). (F) Correlation between OSRG score and TMB. (G) Correlation between OSRG-DEG clusters and TMB. (H) K-M plot analysis was executed to reveal the prognosis of OSRG score and TMB pattern ($P < 0.001$). (I–J) The mutation characteristics of top 20 genes in BC with high OSRG score (I) and OSRG score (J). *** represent $P < 0.001$.

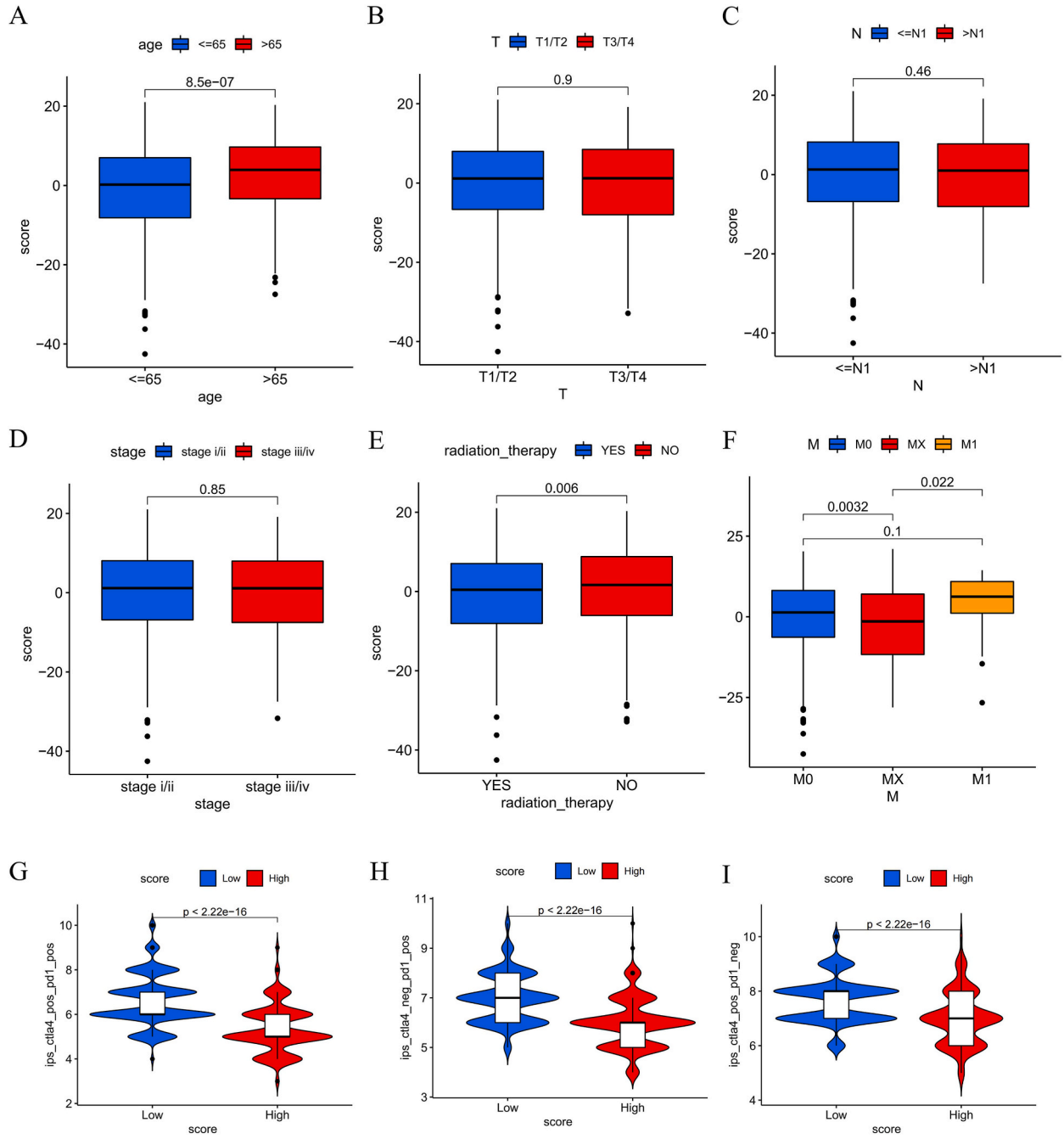

Fig. 6. The correlation between OSRG score and clinical characteristics of BC. (A) The OSRG score of BC patients with different ages. (B) OSRG score in patients with different tumor (T) sizes. (C) OSRG score in patients with different Node-metastasis (N) stages. (D) OSRG score in patients with different tumor stages(E) OSRG score in patients receiving or not receiving radiation therapy. (F) OSRG score in patients with different Metastasis (M) stage. (G–I) Low OSRG score perform a better immune response to IPS-CTLA4-pos-PD1-pos group (G), IPS-CTLA4-neg-PD1-pos group (H) and IPS-CTLA4-pos-PD1-neg group (I).

3.6. The association between OSRG score and clinical characteristics in BC

Next, we investigated the OSRG scores among different subgroups based on TCGA-BRCA clinical data such as gender and tumor stage. The analysis revealed higher OSRG scores in older patients (Fig. 6A). Interestingly, the OSRG score did not exhibit significant differentiation across tumor size, lymph node metastasis, and stage (Fig. 6B–D). Patients who had been clinically treated with radiotherapy had lower OSRG scores (Fig. 6E), and the OSRG score was significantly correlated with tumor metastasis (Fig. 6F). Subsequently, an analysis was conducted on BC patients who underwent PD-L1 and CLTA4 immunotherapy, revealing that the low CRG score group exhibited heightened sensitivity to immunotherapy (Fig. 6G–I). The OSRG score appears to be intricately linked to the efficacy of clinical immunotherapy in BC patients.

Utilizing the R "rms" package, a nomogram was developed to assess the prognostic significance of the OSRG score in BC. Individual scores were assigned to tumor margin, OSRG score, patient age, tumor stage, and other parameters. The individual score denotes the corresponding value of each factor within distinct ranges, while the total score signifies the cumulative sum of all individual scores. This total score serves as a predictive indicator for the prognosis of BC patients at 1, 3, and 5 years (Fig. 7A). The calibration plot validates the robust predictive efficacy of the developed nomogram (Fig. 7B). The predictive utility of the OSRG score in BC patients was demonstrated by evaluating its predictive advantage using ROC curves (Fig. S10).

4. Discussion

BC comprises 30 % of all female cancers and remains one of the most prevalent malignant tumors, with its incidence on the rise over the past decade [18]. Therefore, the development of a tool to aid in the clinical diagnosis and treatment strategy of BC holds significant

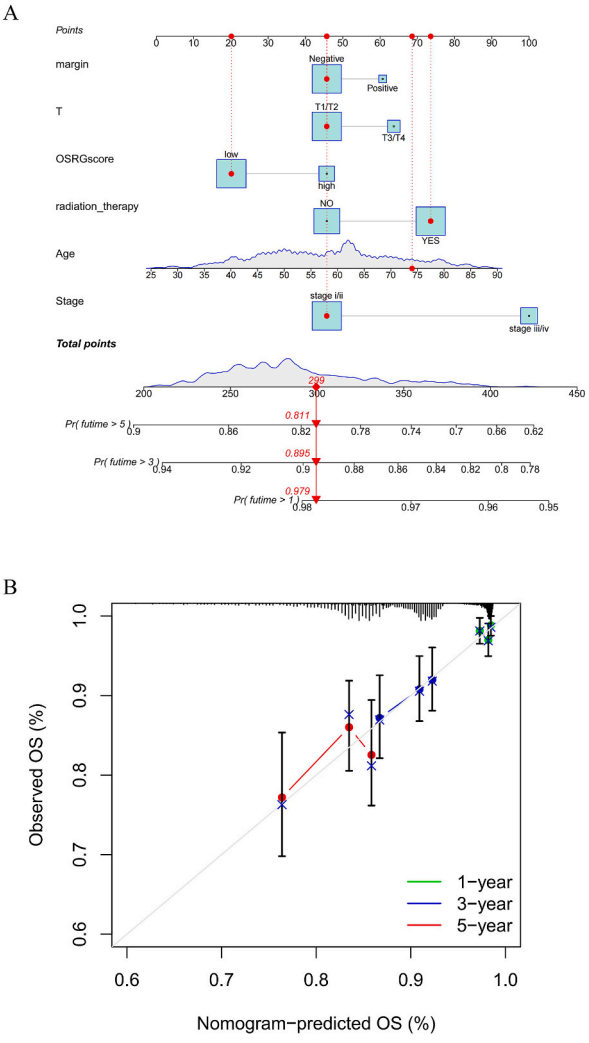

Fig. 7. Generation a nomogram model for BC. (A) The nomogram is on the ground of margin, Tumor size, OSRG score, radiation therapy status, age and tumor stage to predict the OS related prognosis within 5 years. (B) The 1-year, 3-years and 5-years calibration curves of the nomogram.

importance.

ROS are generated by the mitochondrial respiratory chain [19], and an overabundance of ROS has been associated with the development and advancement of several malignant tumors, such as BC [20–23]. The metabolic phenotype of tumor cells is significantly influenced by ROS, which also play a crucial role in regulating tumor growth in a manner that is dependent on the dosage. In the initial phases of tumor formation, minimal quantities of ROS can engage in tumor cell communication and promote tumor cell proliferation, growth, invasion, and metastasis. Nevertheless, during the advanced phases of tumor progression, the accumulation of elevated amounts of ROS within cancerous cells can result in cell cycle arrest or even cell death. This can be attributed to the increased nutritional demands and metabolic disturbances associated with aberrant proliferation [24,25]. It can be inferred that OS plays a pivotal role in the development and advancement of tumors. Hence, it is crucial to possess a thorough comprehension of the interaction between OSRG and various aspects of malignancies in order to guide clinical approaches for tumor detection and treatment. Nevertheless, there is a dearth of models available to forecast the progression of BC patients and provide guidance for appropriate treatment approaches through the creation of OSRG prediction signals.

This study aimed to construct an OSRG model for the purpose of predicting its function in BC. A total of 29 OSRGs were selected for further research based on the examination of the GSEA database. Notable disparities in the expression of the majority of OSRG were detected between BC and normal tissues, suggesting a strong correlation between OSRG and BC. The survival of BC patients was found to be influenced by both the OSRG cluster and the OSRG-DEG cluster. We developed a PCA-based OSRG scoring system to methodically assess the significance of OSRG in BC. Survival analysis revealed a significant association between low OSRG score and better prognosis in BC. The examination of the relationship between 13 immune checkpoint sites and OSRG score revealed a notable increase in the expression of all genes connected to immune checkpoints in the group with a high OSRG score. This finding serves as a foundation for clinical immunotherapy in BC. A nomogram was constructed in order to assess the prognostic significance of the OSRG score in BC, and the examination of calibration plots provided evidence of its predictive effectiveness.

A multifaceted interaction between BC and the immune system has been observed [26]. BC is composed of tumor cells and the TME, which encompasses immune cells, endothelial cells, and stromal cells that engage in mutual interactions [27]. The immunological microenvironment of BC has several components such as lymphocytes, macrophages, natural killer (NK) cells, dendritic cells (DC), myeloid-derived suppressor cells (MDSC), and other variables that mediate the immune response [28]. Cells and immunological factors play a crucial role in expediting the progression of BC by inducing persistent inflammation, hence exerting a substantial impact on the malignant biological processes of cancer cells [29,30]. Improved overall survival and disease-free survival in BC have been found to be associated with higher levels of $CD8^+$ tumor-infiltrating lymphocytes (TIL) and activated NK cells [31,32]. Conversely, the presence of higher regulatory T cells (Treg) infiltration has been linked to lower survival outcomes [33]. The immune system has a crucial role in influencing the advancement of tumors, the response to treatment, and the prognosis of patients. It has the capacity to significantly alter the diagnosis, prognosis, and treatment of BC [34].

Elevated ROS in TME is one of the characteristics of chronic inflammation, and the dynamic changes of this OS mediator form crosstalk with the changes of TIL, thereby affecting the immune response results of BC, and then affecting the occurrence and development of BC [35,36]. Our analysis confirmed the association between OSRG and immune cell infiltration in BC, highlighting the significance of both OSRG and OSRG-DEG in the immune landscape of BC. Further investigation of the OSRG score in the TME of BC showed that high OSRG score corresponded to high expression of all selected important immune checkpoint related genes, underscoring the pivotal role of OS in modulating immune cell infiltration in BC.

The modulation of immune responses is facilitated by immunological checkpoints, which are surface receptors found on immune cells, which can either activate or inhibit these responses [37]. Immunotherapy represented by immune checkpoint inhibitors (CI) has a good therapeutic prospect. The significance of programmed cell death protein 1 (PD-1) and cytotoxic T-lymphocyte-associated antigen 4 (CTLA-4) as crucial targets in BC has been widely investigated [38]. Nevertheless, despite the progressive implementation of CI therapy in the therapeutic management of BC, its effectiveness varies among patients [39]. Therefore, identifying predictive markers for BC patient response to immunotherapy is essential for further advancements in this field. The findings of our study indicate that BC patients with a higher OSRG score exhibited reduced responsiveness to PD-1 and CTLA-4 in comparison to those with lower OSRG scores. This suggests that the OSRG score has the potential to be a useful predictor of immunotherapy outcomes.

However, our study has certain limitations. Firstly, relying on a single data source may introduce bias, necessitating external validation from other datasets to assess the generalizability of the OSRG score. Secondly, the precise mechanisms through which these OSRGs operate in BC require further investigation. Moreover, future research should delve into the specificity of OS and immune cell infiltration in BC to better elucidate the role of OSRG in the TME. Despite these limitations, our developed OSRG signature model effectively predicts BC prognosis and can inform clinical decision-making. A comprehensive analysis of diverse OS patterns in BC will enhance our understanding of immune cell infiltration in TME and facilitate the development of more targeted immunotherapy strategies.

Funding

This work was supported by Shanghai Tenth People's Hospital (No. YNCR2B008).

Data availability statement

Publicly available datasets were analyzed in this study. This data can be found here: GSEA database (https://www.gsea-msigdb.org/gsea/msigdb/human/geneset/GOBP_RESPONSE_TO_OXIDATIVE_STRESS); The Cancer Genome Atlas (TCGA) database

(https://portal.gdc.cancer.gov) and the International Cancer Genome Consortium (ICGC, https://dcc.icgc.org/).

CRediT authorship contribution statement

Diya Liu: Writing – review & editing, Writing – original draft, Visualization, Validation, Methodology, Data curation. **Lin Fang:** Project administration, Investigation, Funding acquisition, Conceptualization.

Declaration of competing interest

The authors declare that they have no known competing financial interests or personal relationships that could have appeared to influence the work reported in this paper.

Acknowledgements

The authors would like to acknowledge the helpful comments on this paper received from the editors and reviewers.

Appendix A. Supplementary data

Supplementary data to this article can be found online at https://doi.org/10.1016/j.heliyon.2024.e34046.

References

[1] H. Sung, J. Ferlay, R.L. Siegel, M. Laversanne, I. Soerjomataram, A. Jemal, F. Bray, Global cancer statistics 2020: GLOBOCAN estimates of incidence and mortality worldwide for 36 cancers in 185 countries, CA A Cancer J. Clin. 71 (3) (2021) 209–249.
[2] R.L. Siegel, K.D. Miller, N.S. Wagle, A. Jemal, Cancer statistics, 2023, CA A Cancer J. Clin. 73 (1) (2023) 17–48.
[3] P. Tsvetkov, S. Coy, B. Petrova, M. Dreishpoon, A. Verma, M. Abdusamad, J. Rossen, L. Joesch-Cohen, R. Humeidi, R.D. Spangler, et al., Copper induces cell death by targeting lipoylated TCA cycle proteins, Science 375 (6586) (2022) 1254–1261.
[4] H.J. Forman, H. Zhang, Targeting oxidative stress in disease: promise and limitations of antioxidant therapy, Nat. Rev. Drug Discov. 20 (9) (2021) 689–709.
[5] H. Sies, D.P. Jones, Reactive oxygen species (ROS) as pleiotropic physiological signalling agents, Nat. Rev. Mol. Cell Biol. 21 (7) (2020) 363–383.
[6] J.D. Hayes, A.T. Dinkova-Kostova, K.D. Tew, Oxidative stress in cancer, Cancer Cell 38 (2) (2020) 167–197.
[7] D. Trachootham, J. Alexandre, P. Huang, Targeting cancer cells by ROS-mediated mechanisms: a radical therapeutic approach? Nat. Rev. Drug Discov. 8 (7) (2009) 579–591.
[8] J. Kim, J. Kim, J.S. Bae, ROS homeostasis and metabolism: a critical liaison for cancer therapy, Exp. Mol. Med. 48 (11) (2016) e269.
[9] P.L. de Sá Junior, D.A.D. Câmara, A.S. Porcacchia, P.M.M. Fonseca, S.D. Jorge, R.P. Araldi, A.K. Ferreira, The roles of ROS in cancer heterogeneity and therapy, Oxid. Med. Cell. Longev. 2017 (2017) 2467940.
[10] A. Sawant, C.C. Schafer, T.H. Jin, J. Zmijewski, H.M. Tse, J. Roth, Z. Sun, G.P. Siegal, V.J. Thannickal, S.C. Grant, et al., Enhancement of antitumor immunity in lung cancer by targeting myeloid-derived suppressor cell pathways, Cancer Res. 73 (22) (2013) 6609–6620.
[11] Q. Meng, D. Catchpoole, D. Skillicorn, P.J. Kennedy, DBNorm: normalizing high-density oligonucleotide microarray data based on distributions, BMC Bioinf. 18 (1) (2017) 527.
[12] A.M. Newman, C.L. Liu, M.R. Green, A.J. Gentles, W. Feng, Y. Xu, C.D. Hoang, M. Diehn, A.A. Alizadeh, Robust enumeration of cell subsets from tissue expression profiles, Nat. Methods 12 (5) (2015) 453–457.
[13] G. Yu, L.G. Wang, Y. Han, Q.Y. He, clusterProfiler: an R package for comparing biological themes among gene clusters, OMICS 16 (5) (2012) 284–287.
[14] M.D. Wilkerson, D.N. Hayes, ConsensusClusterPlus: a class discovery tool with confidence assessments and item tracking, Bioinformatics 26 (12) (2010) 1572–1573.
[15] C. Sotiriou, P. Wirapati, S. Loi, A. Harris, S. Fox, J. Smeds, H. Nordgren, P. Farmer, V. Praz, B. Haibe-Kains, et al., Gene expression profiling in breast cancer: understanding the molecular basis of histologic grade to improve prognosis, J. Natl. Cancer Inst. 98 (4) (2006) 262–272.
[16] D. Zeng, M. Li, R. Zhou, J. Zhang, H. Sun, M. Shi, J. Bin, Y. Liao, J. Rao, W. Liao, Tumor microenvironment characterization in gastric cancer identifies prognostic and immunotherapeutically relevant gene signatures, Cancer Immunol. Res. 7 (5) (2019) 737–750.
[17] A. Mayakonda, D.C. Lin, Y. Assenov, C. Plass, H.P. Koeffler, Maftools: efficient and comprehensive analysis of somatic variants in cancer, Genome Res. 28 (11) (2018) 1747–1756.
[18] Z. Chen, L. Xu, W. Shi, F. Zeng, R. Zhuo, X. Hao, P. Fan, Trends of female and male breast cancer incidence at the global, regional, and national levels, 1990-2017, Breast Cancer Res. Treat. 180 (2) (2020) 481–490.
[19] D.P. Jones, Radical-free biology of oxidative stress, Am. J. Physiol. Cell Physiol. 295 (4) (2008) C849–C868.
[20] H. Zhou, J. Li, Y. He, X. Xia, J. Liu, H. Xiong, SLC25A17 inhibits autophagy to promote triple-negative breast cancer tumorigenesis by ROS-mediated JAK2/STAT3 signaling pathway, Cancer Cell Int. 24 (1) (2024) 85.
[21] Y. Hou, H. Wang, J. Wu, H. Guo, X. Chen, Dissecting the pleiotropic roles of reactive oxygen species (ROS) in lung cancer: from carcinogenesis toward therapy, Med. Res. Rev. 44 (4) (2024) 1566–1595.
[22] H. Im, H.J. Baek, E. Yang, K. Kim, S.K. Oh, J.S. Lee, H. Kim, J.M. Lee, ROS inhibits RORα degradation by decreasing its arginine methylation in liver cancer, Cancer Sci. 114 (1) (2023) 187–200.
[23] Z.P. Germon, J.R. Sillar, A. Mannan, R.J. Duchatel, D. Staudt, H.C. Murray, I.J. Findlay, E.R. Jackson, H.P. McEwen, A.M. Douglas, et al., Blockade of ROS production inhibits oncogenic signaling in acute myeloid leukemia and amplifies response to precision therapies, Sci. Signal. 16 (778) (2023) eabp9586.
[24] N. Aykin-Burns, I.M. Ahmad, Y. Zhu, L.W. Oberley, D.R. Spitz, Increased levels of superoxide and H2O2 mediate the differential susceptibility of cancer cells versus normal cells to glucose deprivation, Biochem. J. 418 (1) (2009) 29–37.
[25] S. Rodic, M.D. Vincent, Reactive oxygen species (ROS) are a key determinant of cancer's metabolic phenotype, Int. J. Cancer 142 (3) (2018) 440–448.
[26] V. Salemme, G. Centonze, F. Cavallo, P. Defilippi, L. Conti, The crosstalk between tumor cells and the immune microenvironment in breast cancer: implications for immunotherapy, Front. Oncol. 11 (2021) 610303.
[27] Y. Zhou, H. Wang, Y. Luo, B. Tuo, X. Liu, T. Li, Effect of metabolism on the immune microenvironment of breast cancer, Biochim. Biophys. Acta Rev. Canc 1878 (2) (2023) 188861.
[28] X. Jiang, D.J. Shapiro, The immune system and inflammation in breast cancer, Mol. Cell. Endocrinol. 382 (1) (2014) 673–682.
[29] J.N. Amens, G. Bahçecioglu, P. Zorlutuna, Immune system effects on breast cancer, Cell. Mol. Bioeng. 14 (4) (2021) 279–292.

[30] X. Lei, Y. Lei, J.K. Li, W.X. Du, R.G. Li, J. Yang, J. Li, F. Li, H.B. Tan, Immune cells within the tumor microenvironment: biological functions and roles in cancer immunotherapy, Cancer Lett. 470 (2020) 126–133.
[31] R. Li, L. Cao, The role of tumor-infiltrating lymphocytes in triple-negative breast cancer and the research progress of adoptive cell therapy, Front. Immunol. 14 (2023) 1194020.
[32] B. Wang, Q. Wang, Z. Wang, J. Jiang, S.C. Yu, Y.F. Ping, J. Yang, S.L. Xu, X.Z. Ye, C. Xu, et al., Metastatic consequences of immune escape from NK cell cytotoxicity by human breast cancer stem cells, Cancer Res. 74 (20) (2014) 5746–5757.
[33] B.R. McRitchie, B. Akkaya, Exhaust the exhausters: targeting regulatory T cells in the tumor microenvironment, Front. Immunol. 13 (2022) 940052.
[34] H. Gonzalez, C. Hagerling, Z. Werb, Roles of the immune system in cancer: from tumor initiation to metastatic progression, Genes Dev. 32 (19–20) (2018) 1267–1284.
[35] L.M. Coussens, Z. Werb, Inflammation and cancer, Nature 420 (6917) (2002) 860–867.
[36] G. Valacchi, F. Virgili, C. Cervellati, A. Pecorelli, OxInflammation: from subclinical condition to pathological biomarker, Front. Physiol. 9 (2018) 858.
[37] K. Esfahani, L. Roudaia, N. Buhlaiga, S.V. Del Rincon, N. Papneja, W.H. Miller Jr., A review of cancer immunotherapy: from the past, to the present, to the future, Curr. Oncol. 27 (Suppl 2) (2020) S87–s97.
[38] S.K. Wong, K.E. Beckermann, D.B. Johnson, S. Das, Combining anti-cytotoxic T-lymphocyte antigen 4 (CTLA-4) and -programmed cell death protein 1 (PD-1) agents for cancer immunotherapy, Expet Opin. Biol. Ther. 21 (12) (2021) 1623–1634.
[39] A.M. Basudan, The role of immune checkpoint inhibitors in cancer therapy, Clin. Pract. 13 (1) (2022) 22–40.